Quantum Electronics **34** (4) 361 – 370 (2004)

OPTICAL WAVEGUIDES

PACS numbers: 07.79.Fc; 42.79.Gn
DOI: 10.1070/QE2004v034n04ABEH002681

Spatial distribution of light fields in a silicon conical waveguide

T.I. Kuznetsova, V.S. Lebedev

Abstract. **The spatial distribution of monochromatic light fields is studied in a tapered silicon fibre with the subwavelength aperture. The lowest-order electric TM_{01} mode is analysed theoretically in a cone with perfectly reflecting metal walls filled with a light absorbing medium. Exact formulas and approximate expressions are obtained for a medium with the complex permittivity, which describe the spatial dependences of the electric and magnetic energy densities inside the cone. The behaviour of the field at the waveguide exit is analysed for the aperture diameter as small as $\sim 1/30$ of the wavelength. The main attention is devoted to the transmission coefficients of the probe, which were calculated for a wide range of its geometrical parameters in the wavelength region from 400 to 830 nm. It is found that silicon provides a substantial increase in the output light energy density at the optical probe end both in the IR and visible spectral regions compared to glass.**

Keywords: *scanning microscopy, near-field optics, tapered waveguide, silicon, dissipative medium, transmission coefficient*.

1. Introduction

Metallised tapered optical waveguides with the subwavelength aperture have received wide applications in near-field scanning optical microscopy. The results of earlier studies in this field are reported in Refs [1 – 3]. The propagation of light in optical probes with glass or silica cores has been recently studied in many experimental papers (see, for example, papers [4 – 8], review [9], and references therein). These investigations were aimed at obtaining high-quality images of nanometre structures. This requires the high degree of localisation of light fields with rather high energy densities. The main problem consists in the increase in the transmission coefficient of optical probes and the achievement of a high spatial resolution.

The behaviour of light fields in tapered optical fibres was studied in a number of theoretical works. Thus, transmission of the 488-nm radiation in glass probes with a small exit aperture (~ 20 nm) providing a small size of the region of localisation of light fields in the near-field zone was studied in Refs [10 – 12]. Numerical calculations were performed in Refs [10 – 12] by the multiple multipole method. Fibres with metal inclined walls and open ends [10, 11] and tapered fibres completely covered by a metal layer whose thickness drastically decreased at the probe end [12] were studied. A specific feature of the second variant [12] is the possibility of exciting surface plasmon modes and the transmission of light through a thin metal layer at the fibre exit, which increase the resulting transmission coefficient of the system. The numerical simulation of the distribution of light fields in optical probes with the subwavelength aperture was also used in some papers (see, for example, Refs [6, 13 – 15]) to determine their optimal shape and geometrical parameters.

A simple method for calculating the spatial distribution of the electromagnetic energy density along the longitudinal coordinate in tapered fibres with perfectly reflecting walls and an open aperture was proposed in Ref. [16]. The results obtained in Ref. [16] are based on the numerical solution of two coupled differential equations for amplitudes of the incident and reflected waves in a supercritical waveguide. The results [16] are applied to the description of light fields with a plane wave front when the waveguide walls make a small angle with its axis.

The spatial characteristics of light waves in a circular tapered waveguide with the subwavelength aperture were investigated in papers [17, 18]. The method to analyse light fields with a plane wave front was developed, which is based on the use of transverse modes parametrically depending on the longitudinal coordinate z. The infinite-order exact system of equations was obtained for the field, which takes into account the waves with all the transverse indices and their mutual interaction. When the wall inclination with respect to the waveguide axis is small, a simplified variant follows from this system of equations in which independent modes exist (as in a cylindrical waveguide). This corresponds to the adiabatic approximation when the waveguide radius $a(z)$ slowly varies along the z axis. It was shown recently [19] that, by using the perturbation theory, the method [17, 18] allows one to obtain a simple system of two coupled equations [16] as the first approximation in the steepness of the waveguide wall inclination. The authors of Refs [17 – 19] also developed the method for describing independent modes taking into account the higher-order terms in the derivative of the waveguide radius with respect

T.I. Kuznetsova, V.S. Lebedev P.N. Lebedev Physics Institute, Russian Academy of Sciences, Leninskii prosp. 53, 119991 Moscow, Russia; e-mail: tkuzn@sci.lebedev.ru; vlebedev@sci.lebedev.ru

Received 15 August 2003; revision received 29 January 2004
Kvantovaya Elektronika **34** (4) 361 – 370 (2004)
Translated by M.N. Sapozhnikov

to z ($a^{-1}\mathrm{d}a/\mathrm{d}z$) and studied transformations of the fundamental wave into higher-order waves.

A great attention was paid in Refs [17 – 19] to the analytic and numerical study of the structure of electric and magnetic fields in a tapered waveguide of a special profile ('hypergeometrical' waveguide). The region of values of the waveguide parameters was found where the amplitudes of all the modes, except the lowest one, are small and the adiabatic approximation provides a high accuracy. For these parameters, the dependence of the transmission coefficient of the system on the characteristics of input radiation and the steepness of the waveguide profile was obtained.

The methods used in Refs [16] and [17 – 19] allow one to elucidate a number of important features in the behaviour of light fields in metallised optical probes with the subwavelength aperture. However, their application is restricted by the region of geometric parameters of the system and wavelengths where the transmission coefficients are small. The numerical calculations [10 – 12] of the transmission coefficients at 488 nm also use a restricted set of parameters of such probes. To move to the region of parameters where the optimal transmission of optical probes is expected, a new approach was developed recently [20, 21] for the description of the light fields both in the waveguide itself and in the near-field zone beyond its subwavelength aperture. The approach uses the modes of the cone with perfectly conducting metal walls and permits the investigation of the spatial structure of waves with a spherical wave front and the calculation of the transmission coefficient of such probes. A peculiarity related to the subwavelength size of the exit aperture was taken into account in Refs [20, 21] by choosing proper solutions – standing waves with amplitudes drastically decreasing as the cone apex is approached. This method allows one to solve the problem exactly, so that the restrictions on the steepness of the waveguide profile were eliminated in Refs [20, 21].

In all the above papers, the light fields were considered in optical probes with glass waveguide cores. The refractive index n of glass in the optical range very weakly depends on frequency and is ~ 1.5, while absorption is virtually absent. It is obvious that an increase in the refractive index n of a medium should lead to an increase in the transmission coefficient of light in the probe because of a decrease in the wavelength in its core ($\lambda_c = \lambda/n$, where λ is the wavelength of light in vacuum). Therefore, the length of the supercritical region of a tapered waveguide decreases with increasing n, resulting in a drastic decrease in the field attenuation. On the other hand, absorption of light becomes substantial in media with the high refractive index in the visible region. This leads to an additional attenuation of the field propagating in the optical probe. To elucidate the role of these two competing factors, it is necessary to develop the theory of propagation of light in probes filled with a medium with the complex permittivity.

Of special interest for practical applications is analysis of the spatial structure of light fields in optical probes with a silicon core. Already the first experiments [22 – 24] in the IR spectral region have shown that the transmission coefficient of such probes can be substantially increased and the high spatial resolution can be simultaneously achieved. This conclusion is confirmed by the comparative analysis [25] of transmission of IR radiation at 1.3 μm in glass and silicon two-dimensional probes with a small tapering angle. The numerical calculation [25] was performed using a two-dimensional model assuming the absence of absorption in the probe. Note that silicon probes tapering down to the nanometre diameters are also used in apertureless near-field scanning microscopy based on the detection of scattered light [26].

The aim of this paper is to study the propagation of visible and near-IR radiation in tapered optical probes with a silicon core. The theory is developed taking into account the frequency dispersion and absorption of light in the silicon core of the probe. The analytic description of the behaviour of light waves in a tapered probe with perfectly conducting metal walls, which is filled with an absorbing medium with the complex permittivity, is presented in sections 2 and 3. The description was performed for the lowest-order transverse magnetic TM_{01} mode. We analysed the dependences of the energy densities corresponding to different components of the field (E_r, E_θ and H_φ) and of the integrated total energy density W_{tot} on the cone angle and the radial coordinate r measured from the cone apex. Both exact formulas and simple analytic expressions were obtained which describe the drop of the electromagnetic energy density as the cone apex is approached. Asymptotic expressions are also presented which can be applied for values of r exceeding the wavelength.

The developed approach is used in section 4 to study the dependences of the transmission coefficient of an optical silicon probe on its geometrical parameters and the wavelength. The calculations were performed for the 400 – 830-nm wavelength region. A special attention was paid to the study of the effect of absorption of light in silicon on the transmission of the probe in the IR and visible spectral regions. For this purpose, we investigated the dependences of the transmission coefficient on the probe length.

2. Basic expressions for light fields in a medium with the complex permittivity

Let us present basic expressions for electromagnetic fields in a dispersion medium of a cone with perfectly reflecting metal walls. Consider the monochromatic dependence of the fields on time, the factor $\exp(-\mathrm{i}\omega t)$ being omitted below. The initial equation for the Hertz function $U(r, \theta, \varphi)$ of the electromagnetic field in a cone in the spherical coordinate system (r, θ, φ) has the form [27]

$$\frac{\partial^2 U}{\partial r^2} + \frac{1}{r^2}\left[\frac{1}{\sin\theta}\frac{\partial}{\partial\theta}\left(\sin\theta\frac{\partial U}{\partial\theta}\right) + \frac{1}{\sin^2\theta}\frac{\partial 2U}{\partial\varphi^2}\right] + k^2 U = 0, \quad (1)$$

where r is the distance from the cone apex; and θ and φ are the polar and azimuthal angles, respectively. The wave number k in (1) for an absorbing medium is complex:

$$k = \frac{\omega}{c}(\varepsilon\mu)^{1/2}, \quad (\varepsilon\mu)^{1/2} = n + \mathrm{i}\varkappa, \quad (2)$$

where ω and c are the frequency and velocity of light; and n and $\varkappa$ are the refractive index and attenuation coefficient of the medium, respectively. Assuming that the magnetic permeability of the medium is $\mu = 1$, we obtain the relation between the complex permittivity $\varepsilon(\omega) = \varepsilon'(\omega) + \mathrm{i}\varepsilon''(\omega)$ and quantities $n(\omega)$ and $\varkappa(\omega)$ [28]:

$$\varepsilon' \equiv \mathrm{Re}\,\varepsilon = n^2 - \varkappa^2, \quad \varepsilon'' \equiv \mathrm{Im}\,\varepsilon = 2n\varkappa. \quad (3)$$

For the electric waves under study [transverse magnetic (TM) modes], the relations between the field components and the Hertz function have the form [27]

$$E_r = \frac{\partial^2 U}{\partial r^2} + \frac{\omega^2(\varepsilon' + \mathrm{i}\varepsilon'')}{c^2} U, \tag{4}$$

$$E_\theta = \frac{1}{r}\frac{\partial^2 U}{\partial r \partial \theta}, \quad E_\varphi = \frac{1}{r\sin\theta}\frac{\partial^2 U}{\partial r \partial \varphi},$$

$$H_r = 0, \quad H_\theta = -\frac{\mathrm{i}\omega(\varepsilon' + \mathrm{i}\varepsilon'')}{c}\frac{1}{r\sin\theta}\frac{\partial U}{\partial \varphi}, \tag{5}$$

$$H_\varphi = \frac{\mathrm{i}\omega(\varepsilon' + \mathrm{i}\varepsilon'')}{c}\frac{1}{r}\frac{\partial U}{\partial \theta}.$$

The components E_r, E_θ, E_φ and H_r, H_θ, H_φ are the corresponding projections of the electric (***E***) and magnetic (***H***) fields on the axes of the spherical coordinate system r, θ, φ. In this case, the boundary condition has the form $U(r,\theta)|_{\theta=\theta_0} = 0$, where $2\theta_0$ is the cone angle (Fig. 1).

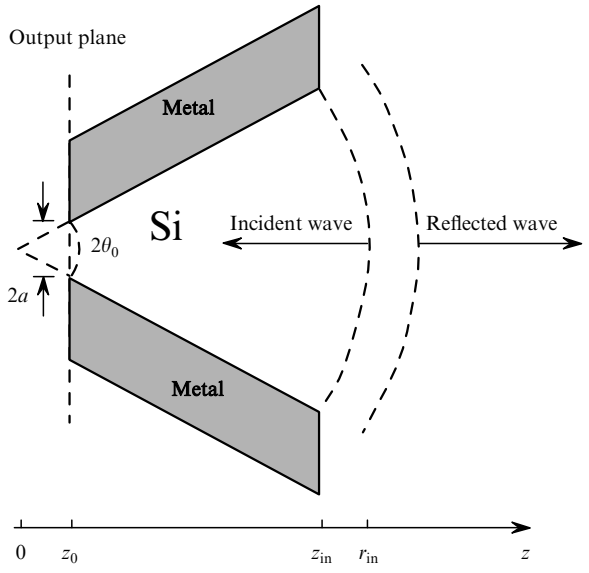

Figure 1. Scheme illustrating propagation of spherical waves in a metallised tapered waveguide with a silicon core: (a) exit aperture radius; ($2\theta_0$) cone angle; (z_{in}) and (z_0) the entry and exit longitudinal coordinates of the waveguide; (r_{in}) radial coordinate at the waveguide entrance ($z_{in} = r_{in}\cos\theta_0$).

For the case of propagation of light through a tapered waveguide with the subwavelength aperture, we will use the exact solution of Eqn (1) corresponding to a standing wave:

$$U(r,\theta,\varphi) = \Re(r) P_\nu^m(\cos\theta)\mathrm{e}^{\mathrm{i}m\varphi}, \tag{6}$$

$$\Re(r) = C r j_\nu\left[(n + \mathrm{i}\varkappa)\frac{\omega r}{c}\right].$$

The dependence of the Hertz function on the polar angle θ in (6) is determined by the adjoined Legendre function of the first kind $P_\nu^m(\cos\theta)$ of power ν and order m [29] (m is an integer). The radial dependence $\Re(r)$ is described by the spherical Bessel function of the first kind $j_\nu(z)$ with the complex argument and the non-integer index ν. C is an arbitrary constant*.

In an absorbing medium ($\varkappa \neq 0$), general expression (6) for the radial part of the Hertz function at large distances from the cone apex ($r \gg 1/|k|$) has the form

$$\Re(r) \approx \frac{C}{2\mathrm{i}}\frac{c}{\omega(n + \mathrm{i}\varkappa)}\left\{\exp\left[(-\varkappa + \mathrm{i}n)\frac{\omega r}{c} - \frac{\mathrm{i}\pi\nu}{2}\right]\right.$$

$$\left. - \exp\left[(\varkappa - \mathrm{i}n)\frac{\omega r}{c} + \frac{\mathrm{i}\pi\nu}{2}\right]\right\}. \tag{7}$$

Asymptotic expression (7) describes a standing wave, which is a superposition of two counterpropagating travelling waves. The ratio of amplitudes of these waves is determined by the exponential factor $\exp(-2\varkappa\omega r/c)$. For a transparent medium (when $\varkappa = 0$), expression (7) takes a very simple form

$$\Re(r) \approx \frac{C}{(n\omega/c)}\sin\left(\frac{n\omega}{c}r - \frac{\pi\nu}{2}\right) \quad [r \gg c/(n\omega)]. \tag{8}$$

The function $\Re(r)$ decreases according to a power law as the cone apex is approached [$r \ll c/(\omega|n + \mathrm{i}\varkappa|)$]:

$$\Re(r) \approx \frac{C\sqrt{\pi}}{2^{\nu+1}\Gamma(\nu + 3/2)}\left[\frac{\omega(n + \mathrm{i}\varkappa)}{c}\right]^\nu r^{\nu+1}. \tag{9}$$

Taking the specific form of the Hertz function (6) into account, the boundary condition for TM waves can be written in terms of the adjoined Legendre function of the first kind: $P_\nu^m(\cos\theta_0) = 0$. This condition determines a set of eigenvalues ν_{mn} ($m = 0, 1, 2, ...$, $n = 1, 2, 3, ...$). Each choice of a pair of numbers m and n specifies certain TM_{mn} modes of the field. The eigenvalues ν_{mn} obtained in this case depend on the cone angle $2\theta_0$, the value of ν_{mn} increasing with decreasing θ_0. For example, for $\theta_0 = \pi/2$, $\pi/3$, $\pi/4$, and $\pi/6$, the eigenvalues for the lowest-order TM_{mn} mode with $n = 1$ and $m = 0$, are 1, 1.777, 2.548, and 4.083, respectively.

In this paper, we consider the behaviour of the fundamental electric TM_{01} mode in a dispersion medium of the cone. In this case $\partial U/\partial\varphi = 0$, so that, according to expressions (4)–(6), there exist only three nonzero components of the field: E_r, E_θ and H_φ. By substituting (6) into (4) and (5), we obtain

$$E_r = \frac{\nu(\nu+1)}{r^2}\Re(r)P_\nu(\cos\theta), \quad E_\theta = \frac{1}{r}\frac{\partial\Re(r)}{\partial r}\frac{\partial P_\nu(\cos\theta)}{\partial\theta}, \tag{10}$$

$$H_\varphi = \mathrm{i}\frac{\omega(\varepsilon' + \mathrm{i}\varepsilon'')}{c}\frac{1}{r}\Re(r)\frac{\partial P_\nu(\cos\theta)}{\partial\theta}, \tag{11}$$

*Note that the Hertz function in a cone filled with a transparent glass ($\varkappa = 0$) was expressed in our paper [20] in terms of the usual Bessel function $J_{\nu+1/2}(x)$ rather than in terms of the spherical Bessel function $j_\nu(x) = (\pi/2x)^{1/2}J_{\nu+1/2}(x)$, as in (6). Therefore, constants C in Ref. [20] and here differ by the factor $[\pi c/(2\omega\sqrt{\bar{\varepsilon}})]^{1/2}$.

where $P_v(\cos\theta)$ is the Legendre function of the first kind of power v [29].

3. Field energy density in a dissipative medium

In a dissipative medium with the complex permittivity (3) and magnetic permeability $\mu = \mu' + i\mu''$, the general expression for the time-averaged electromagnetic energy density (see, for example, Ref. [28]) leads to the relations

$$w_r = \frac{1}{16\pi}\frac{d(\omega\varepsilon')}{d\omega}|E_r|^2, \quad w_\theta = \frac{1}{16\pi}\frac{d(\omega\varepsilon')}{d\omega}|E_\theta|^2, \quad w_\varphi = \frac{1}{16\pi}\frac{d(\omega\mu')}{d\omega}|H_\varphi|^2. \tag{12}$$

for the radial (w_r), polar (w_θ), and azimuthal (w_φ) components of the field energy density, respectively.

To find the transmission coefficient of a tapered waveguide, we introduce, according to Ref. [20], integrals from quantities w_r, w_θ, and w_φ over the surface of the sphere of radius r within the cone (see Fig. 1):

$$W_\beta = 2\pi r^2 \int_0^{\theta_0} w_\beta(r,\theta)\sin\theta d\theta \qquad (\beta = r,\theta,\varphi). \tag{13}$$

We will call these quantities the integrated energy densities. The resulting equations for W_r, W_θ, and W_φ explicitly dependent on the radial coordinate r can be obtained from expressions (10)–(13) using expression (6) for the Hertz function. In this case, the integrated energy density W_r takes the form

$$W_r(r) = \frac{|C|^2}{8}\frac{d(\omega\varepsilon')}{d\omega}[v(v+1)]^2\mathfrak{I}_v^{(1)}\left|j_v\left[(n+i\varkappa)\frac{\omega r}{c}\right]\right|^2, \tag{14}$$

$$\mathfrak{I}_v^{(1)}(\theta_0) = \int_0^{\theta_0}[P_v(\cos\theta)]^2\sin\theta d\theta. \tag{15}$$

The angular integral $\mathfrak{I}_v^{(1)}$ in (14) depends on the cone angle $2\theta_0$. The expression for the polar component W_θ can be obtained using the known relation for the derivative of the spherical Bessel function. This gives

$$W_\theta(r) = \frac{|C|^2}{8}\frac{d(\omega\varepsilon')}{d\omega}\mathfrak{I}_v^{(2)}\left|(v+1)j_v\left[(n+i\varkappa)\frac{\omega r}{c}\right] - \left[(n+i\varkappa)\frac{\omega r}{c}\right]j_{v+1}\left[(n+i\varkappa)\frac{\omega r}{c}\right]\right|^2, \tag{16}$$

where the angular integral is

$$\mathfrak{I}_v^{(2)}(\theta_0) = \int_0^{\theta_0}\left[\frac{\partial P_v(\cos\theta)}{\partial\theta}\right]^2\sin\theta d\theta = v(v+1)\mathfrak{I}_v^{(1)}(\theta_0). \tag{17}$$

Similarly, using expressions (10)–(13) and (6), we obtain the expression for the component $W_\varphi(r)$:

$$W_\varphi(r) = \frac{|C|^2|\varepsilon' + i\varepsilon''|^2}{8}\left(\frac{\omega r}{c}\right)^2\mathfrak{I}_v^{(2)}\left|j_v\left[(n+i\varkappa)\frac{\omega r}{c}\right]\right|^2. \tag{18}$$

By summing expressions (14), (16), and (18), we obtain the total integrated density of the electromagnetic field energy inside the cone:

$$W_{tot}(r) = 2\pi r^2\int_0^{\theta_0}(w_r + w_\theta + w_\varphi)\sin\theta d\theta = W_r(r) + W_\theta(r) + W_\varphi(r). \tag{19}$$

It is interesting to study the asymptotic behaviour of the integrated energy densities for the electric ($W_{el} = W_r + W_\theta$) and magnetic ($W_m = W_\varphi$) components of the field at large distances r from the cone: $r \to \infty$. The corresponding expressions follow directly from general expressions (14)–(18) by using the asymptotic expression for the spherical Bessel function $j_v(z)$ with the complex argument. As a result, we obtain for $W_{el}(r)$ at $r \gg c/(\omega|n+i\varkappa|)$ the expression

$$W_{el} = \frac{|C|^2}{16}\frac{d(\omega\varepsilon')}{d\omega}\mathfrak{I}_v^{(2)} \times\left[\cosh\left(2\varkappa\frac{\omega r}{c}\right) + \cos\left(2n\frac{\omega r}{c} - \pi v\right)\right]. \tag{20}$$

A similar asymptotic expression for the integrated magnetic energy density W_m in a dissipative medium of a tapered waveguide has the form

$$W_m = \frac{|C|^2}{16}|\varepsilon' + i\varepsilon''|\mathfrak{I}_v^{(2)} \times\left[\cosh\left(2\varkappa\frac{\omega r}{c}\right) - \cos\left(2n\frac{\omega r}{c} - \pi v\right)\right]. \tag{21}$$

It follows from (20) and (21) that at large radial coordinates r the oscillations of electric and magnetic fields in the tapered waveguide are out of phase. Note also that the term $\cosh(2\varkappa\omega r/c)$ entering the dependences of W_{el} and W_m on r shows the effect of absorption of light in the dissipative medium.

By summing expressions (20) and (21), we obtain the asymptotic expression for the integrated density of the total energy of the field $W_{tot} = W_{el} + W_m$ in the tapered waveguide

$$W_{tot} = \frac{|C|^2}{16}\mathfrak{I}_v^{(2)}\left\{\left[\frac{d(\omega\varepsilon')}{d\omega} + |\varepsilon|\right]\cosh\left(2\varkappa\frac{\omega r}{c}\right) + \left[\frac{d(\omega\varepsilon')}{d\omega} - |\varepsilon|\right]\cos\left(2n\frac{\omega r}{c} - \pi v\right)\right\}. \tag{22}$$

Therefore, the dependence of the integrated density of the total electromagnetic energy $W_{tot}(r)$ on the radial coordinate for $r \gg c/(\omega|n + i\varkappa|)$ exhibits oscillations. These oscillations, which do not disappear with increasing r, are produced due to the permittivity dispersion. They are absent in transparent (dispersionless) media ($\varkappa = 0$, $n =$ const). In this case, asymptotic expressions (20)–(22) are reduced to a very simple form

$$W_{\rm el} = \frac{|C|^2\varepsilon}{8}\mathfrak{I}_\nu^{(2)}\cos^2\left(\frac{n\omega r}{c} - \frac{\pi\nu}{2}\right), \tag{23}$$

$$W_{\rm m} = \frac{|C|^2\varepsilon}{8}\mathfrak{I}_\nu^{(2)}\sin^2\left(\frac{n\omega r}{c} - \frac{\pi\nu}{2}\right),$$

$$W_{\rm tot} = \frac{|C|^2\varepsilon}{8}\mathfrak{I}_\nu^{(2)}, \qquad r \gg c/(n\omega) \tag{24}$$

in accordance with results obtained in Refs. [20, 21].

In the presence of the frequency dispersion of a medium, the amplitudes of oscillations of the energy density of electric [$W_{\rm el} \propto {\rm d}(\omega\varepsilon')/{\rm d}\omega$] and magnetic ($W_{\rm m} \propto |\varepsilon|$) fields in the tapered waveguide are different. Therefore, these oscillations are not mutually compensated upon summation of expressions (20) and (21). The case when the imaginary part of the permittivity of the medium is small $\varepsilon'' \ll \varepsilon'$ (i.e. $\varkappa \ll n$) is most interesting for applications. In this case, the relative amplitude of oscillations of the integrated density of the total energy of the electromagnetic field in the region $r \gg c/(\omega n)$ is determined by the quantity $\gamma = (\omega {\rm d}\varepsilon'/{\rm d}\omega)/(2\varepsilon' + \omega d\varepsilon'/d\omega)$. It is obvious that $\gamma \ll 1$ in the case of a small dispersion: $\omega {\rm d}\varepsilon'/{\rm d}\omega \ll \varepsilon'$. In the opposite limiting case ($\omega {\rm d}\varepsilon'/{\rm d}\omega \gg \varepsilon'$), the value of γ is of the order of unity.

The transmission coefficient is calculated by averaging expression (22) over the period of the oscillating component of the integrated energy density of the electromagnetic field. This gives

$$\overline{W}_{\rm tot} = \frac{|C|^2}{16}\mathfrak{I}_\nu^{(2)}\left[\frac{{\rm d}(\omega\varepsilon')}{{\rm d}\omega} + |\varepsilon|\right]\cosh\left(2\varkappa\frac{\omega r}{c}\right). \tag{25}$$

For a transparent medium ($\varkappa = 0$), this expression transforms to (24).

One should bear in mind that in the presence of energy dissipation in a tapered waveguide, the energy fluxes in the incident wave,

$$S_{\rm in}(r) = \frac{c\overline{W}_{\rm tot}(r)\exp(2\varkappa\omega r/c)}{n[\exp(2\varkappa\omega r/c) + \exp(-2\varkappa\omega r/c)]}, \tag{26}$$

and in the counterpropagating wave reflected from the waveguide walls,

$$S_{\rm r}(r) = -\frac{c\overline{W}_{\rm tot}(r)\exp(-2\varkappa\omega r/c)}{n[\exp(2\varkappa\omega r/c) + \exp(-2\varkappa\omega r/c)]} \tag{27}$$

are different. One can easily see that the ratio of these fluxes is $|S_{\rm r}/S_{\rm in}| = \exp(-4\varkappa\omega r/c)$. Note also that asymptotic expressions (22)–(27) are applied in the region $r \gg c/(\omega|n + i\varkappa|)$. This means that the distance r from the cone apex should exceed the wavelength of light in the medium.

Consider the spatial distribution of the electromagnetic energy in a silicon tapered waveguide with the subwavelength aperture (see Fig. 1). According to Ref. [30], the refractive index $n(\omega)$ of silicon monotonically increases from 3.67 to 5.57 in the region from 1.5 to 3.1 eV (corresponding to the wavelength range from 830 to 400 nm), while the attenuation coefficient $\varkappa(\omega)$ increases from 0.005 to 0.387. In this case, the ratio $\varkappa/n$ increases from 1.4×10^{-3} to 6.9×10^{-2}. Therefore, energy losses caused by absorption of light in silicon are especially large in the visible spectral region, whereas their role in the IR region is insignificant.

Figure 2 shows the radial dependences of the integrated density of the total field energy $W_{\rm tot} = W_r + W_\theta + W_\varphi$ calculated for the fundamental electric TM_{01} wave. The calculations were performed for the cone angle $2\theta_0 = \pi/3$ and wavelengths of light in vacuum equal to 800 and 500 nm (Figs 2a and b, respectively). One can see that these two dependences are qualitatively different.

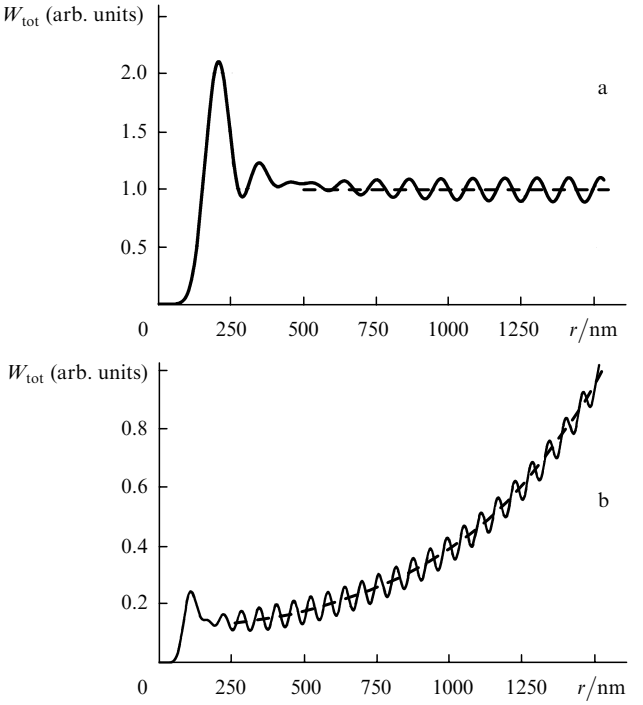

Figure 2. Radial dependences $W_{\rm tot}(r)$ of the total electromagnetic energy density in a silicon cone integrated over the segment $0 \leqslant \theta \leqslant \theta_0$, $0 \leqslant \varphi \leqslant 2\pi$ of a spherical surface. Calculations were performed for the lowest-order TM_{nm} mode ($m = 0$, $n = 1$) for the cone angle $2\theta_0 = 60^\circ$ ($\nu = 4.084$) and wavelengths of light in vacuum equal to 800 (a) and 500 nm (b). Solid curves were calculated by general expressions (14), (16), (18), and (19). Dashed curves are the values of $\overline{W}_{\rm tot}(r)$ averaged over oscillations determined by expression (25).

In the near-IR region at 800 nm, the attenuation coefficient is $\varkappa = 6.1 \times 10^{-3}$ and the refractive index of silicon is $n = 3.69$. It follows from Fig. 2a that the radial dependence $W_{\rm tot}(r)$ for a metallised silicon probe is quite similar to that for a metallised glass probe (cf. Fig. 2 in Ref. [20]). Some differences are related to the presence of weak oscillations in the integrated density of the total energy of the electromagnetic field $W_{\rm tot}$ in silicon (solid curve in Fig. 2a), which do not attenuation with increasing r. The nature of these oscillations in dispersion media was discussed in section 3. The dashed curve in Fig. 2a illustrates the radial dependence of the integrated energy density $\overline{W}_{\rm tot}$ averaged over oscillations in the asymptotic region $r \gg c/(n\omega)$. One can see that, because of a weak attenuation of the field in silicon at 800 nm, the value of $\overline{W}_{\rm tot}$ is almost constant in the region satisfying the condition $c/(n\omega) \ll r \ll c/(\varkappa\omega)$. Therefore, the behaviour of $\overline{W}_{\rm tot}$ in the IR region in a metallised silicon tapered probe shown in

Fig. 2a is similar to that in the case of a transparent glass [20, 21].

The values of $\varkappa$ and n in silicon in the visible region at 500 nm are 7.3×10^{-2} and 4.3, respectively. Therefore, the attenuation coefficient of light increases by an order of magnitude compared to that at 800 nm. This leads to the different dependence $W_{\rm tot}(r)$ in the region $r \gg c/(n\omega)$. One can see from Fig. 2b that, due to absorption of light in the silicon core of the probe, the integrated energy density $W_{\rm tot}(r)$ of the field averaged over spatial oscillations strongly decreases at first as the cone apex is approached from large values of r ($r \gg \lambda_{\rm Si}$; $r = 1500$ nm in the example under study). This occurs down to $r \sim \lambda_{\rm Si}$, where $\lambda_{\rm Si} = \lambda/n_{\rm Si} = 116$ nm is the wavelength of light in silicon for the wavelength of light in vacuum $\lambda = 500$ nm.

As in the previous case (Fig. 2a), the dependence $W_{\rm tot}(r)$ exhibits oscillations even in the asymptotic region, i.e., for $r \gg \lambda_{\rm Si}$. However, due to the increase in the permittivity dispersion of silicon in the visible region (at 500 nm), the amplitude of oscillations of the function $W_{\rm tot}(r)$ strongly increases compared to that for $\lambda = 800$ nm. In the region $r \sim \lambda_{\rm Si}$, the integrated energy density has the peak, and then $W_{\rm tot}(r)$ drastically decreases at $r \ll \lambda_{\rm Si}$ as the cone apex is approached. According to (9), the decrease follows the power law $W_{\rm tot} \propto (|k|r)^{2\nu}$, as in the case of transparent glass core.

As a whole, however, the behaviour of optical fields in the short-wavelength region in a silicon probe substantially differs from that in a glass probe because of a strong attenuation of light waves. The energy dissipation in silicon becomes especially significant when the length $r_{\rm in}$ of the probe generatrix (see Fig. 1) considerably exceeds the characteristic attenuation length $r_\varkappa = c/(2\varkappa\omega)$ of the field ($r_\varkappa = 2.66$, 0.84 and 0.45 μm for $\lambda = 633$, 532, and 488 nm, respectively).

4. Transmission of light in a tapered silicon probe

The study of the dependences of the transmission coefficient of an optical silicon probe on its geometrical parameters and wavelength attracts special interest. In the case of a probe with the subwavelength aperture, it is necessary to distinguish transmission coefficients corresponding to the transmission of incident radiation to the near- and far-field zones (see, for example, Refs [9, 18]). In this paper, we will consider the transmission coefficient allowing the determination of the electromagnetic field in the near-field zone at the probe exit. According to Refs [18–21], such a transmission coefficient T is defined in terms of the integrated energy densities of the field at the probe entrance and exit rather than in terms of energy fluxes (as in the case of propagating waves). In this case, one should bear in mind that the expressions for fields presented in sections 2 and 3 are relevant to the case of a closed metallised cone. The scale of perturbations of the fields caused by the presence of the entrance and exit apertures in an optical probe was estimated in papers [18–21]. It was found that reflection of fields from the exit aperture only slightly changes the amplitude and distribution of light fields calculated for a closed cone under the condition that the aperture diameter d is substantially smaller than the wavelength λ.

The transmission coefficient T for spherical waves is equal to the ratio $W_{\rm tot}^{\rm out}/W_{\rm tot}^{\rm in}$ of the field energy density $W_{\rm tot}^{\rm out} \equiv W_{\rm tot}(z_0)$ at the exit of a truncated cone ($z = z_0$) integrated over a flat aperture of radius a (see Fig. 1),

$$W_{\rm tot}^{\rm out} = 2\pi \int_0^a w_{\rm tot}(\rho, z_0)\rho {\rm d}\rho, \quad a = z_0 \tan\theta_0, \tag{28}$$

$$w_{\rm tot}(\rho, z_0) = w_r(\rho, z_0) + w_\theta(\rho, z_0) + w_\varphi(\rho, z_0) \tag{29}$$

to the integrated density of the total energy $W_{\rm tot}^{\rm in}$ at the probe entrance.

In a dissipative medium, the expression for $W_{\rm tot}^{\rm in}$ should be modified somewhat compared to the case of a transparent medium (cf. Ref. [20]). The quantity $\alpha(r_{\rm in}, \omega)$ should be introduced, which depends on the frequency ω and distance $r_{\rm in}$ from the cone apex to the probe entrance. In this case, the corresponding general expression takes the form

$$W_{\rm tot}^{\rm in} = \alpha 2\pi r_{\rm in}^2 \int_0^{\theta_0} w_{\rm tot}(r_{\rm in}, \theta)\sin\theta {\rm d}\theta, \tag{30}$$

$$\alpha(r_{\rm in}, \omega) = \left| \frac{(n/c)S_{\rm in}(r_{\rm in})}{\overline{W}_{\rm tot}(r_{\rm in})} \right| = \frac{1}{1 + \exp(-4\varkappa\omega r_{\rm in}/c)}. \tag{31}$$

The integration in (30) is performed over the part of a spherical surface inside the cone ($0 \le \theta \le \theta_0$, $0 \le \varphi \le 2\pi$) for $r = r_{\rm in}$. The quantity α is introduced in (30) to take into account in the transmission coefficient T only the part $W_{\rm tot}(r_{\rm in})$ of the integrated field energy density that corresponds to the incident wave, excluding completely the contribution from the reflected wave. The value of α in (31) changes from 1/2 to 1 depending on the attenuation coefficient $\varkappa$ and the length $r_{\rm in}$ of the generatrix of a tapered probe. For a transparent medium ($\varkappa = 0$), we obtain from (31) $\alpha = 1/2$, so that the definition of the transmission coefficient in this particular case [20, 21] coincides with the general definition presented here. In a dissipative medium, $\alpha \to 1$ if the ratio $2\varkappa\omega r_{\rm in}/c$ becomes substantially greater than unity. This behaviour of α is illustrated in Fig. 3 where

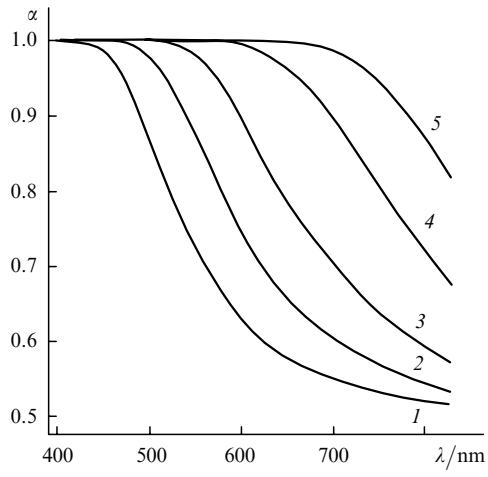

Figure 3. Dependences of α on the wavelength of light in vacuum λ calculated by expression (31) taking into account the dispersion of the attenuation coefficient of light $\varkappa(\lambda)$ in silicon according to data [30] for the radial coordinate $r_{\rm in} = 0.5$ (*1*), 1 (*2*), 2 (*3*), 5 (*4*), and 10 μm (*5*) measured from the cone apex in front of the probe.

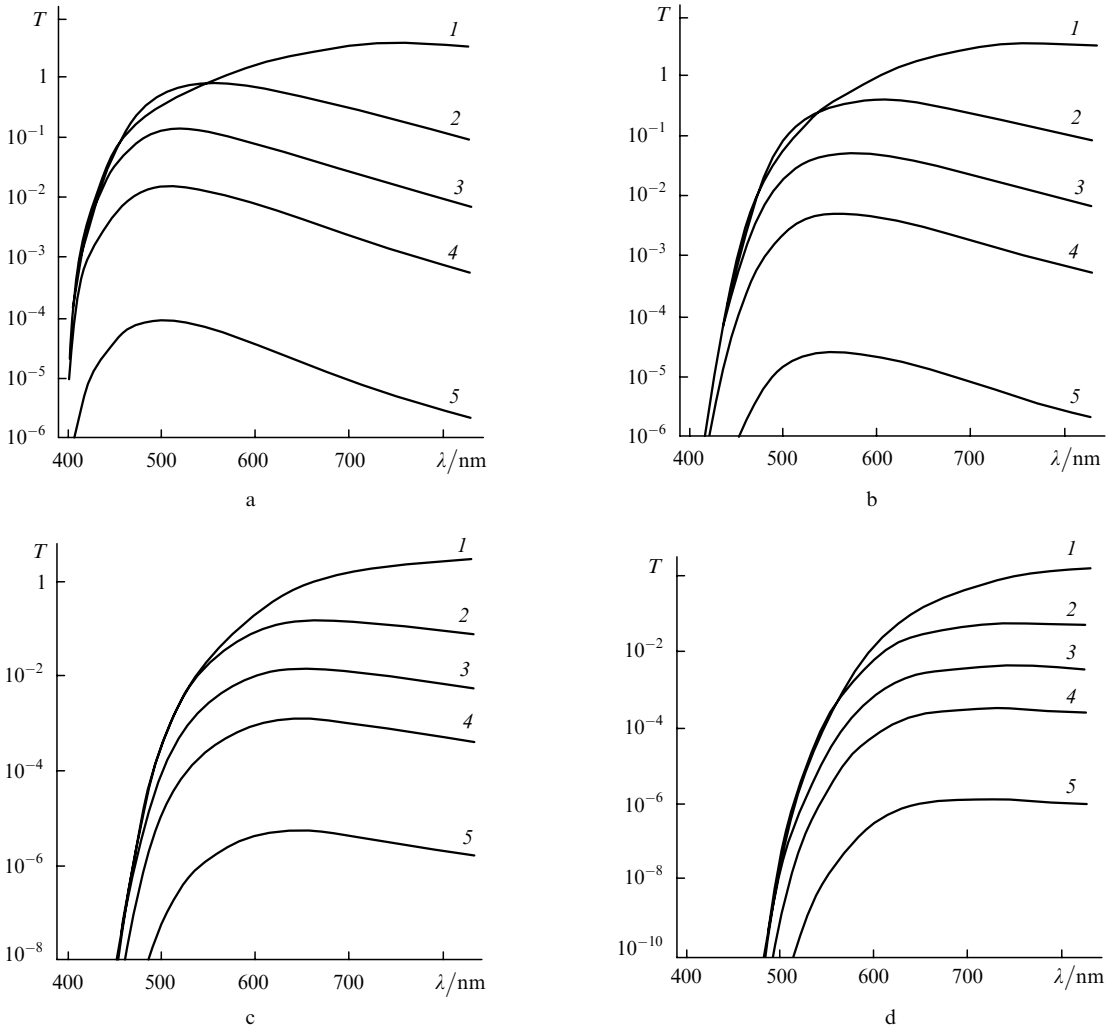

Figure 4. Dependences of the transmission coefficient T of a tapered silicon probe on the wavelength of light in vacuum for distances from the cone apex to the probe entry $r_{in} = 1$ (a), 2 (b), 5 (c), and 10 μm (d). Calculations were performed for the TM_{01} mode, the cone angle $2\theta_0 = 60^\circ$ ($v = 4.084$), and the exit aperture diameter $d = 200$ (*1*), 100 (*2*), 70 (*3*), 50 (*4*), and 25 nm (*5*).

the spectral dependences $\alpha(\lambda)$ are presented for silicon in the wavelength range from 400 to 830 nm for the distance from the cone apex to the probe entrance $r_{in} = 0.5$, 1, 2, 5, and 10 μm.

Figures 4 and 5 show the spectral dependences of the transmission coefficient of a metallised tapered silicon probe calculated for the fundamental TM_{01} wave. The calculations were performed for two angles θ_0 equal to $\pi/6$ (Fig. 4) and $\pi/3$ (Fig. 5) in the wavelength region from 400 to 830 nm. All the spectral dependences were calculated for four values r_{in} equal to 1, 2, 5, and 10 μm. This allows us to study the effect of light absorption in silicon on the transmission coefficient of the system. Curves (*1*), (*2*), (*3*), (*4*), and (*5*) in Figs 4 and 5 were obtained for the exit-aperture diameters equal to 200, 100, 70, 50, and 25 nm, respectively.

One can see from Figs 4 and 5 that the transmission coefficient T of the probe strongly depends on the aperture diameter d. The transmission coefficient T drastically decreases with decreasing diameter d, whose values 100, 70, 50, and 25 nm correspond to the supercritical regime of the waveguide. The case $d = 200$ nm is distinguished among the examples studied. This is explained by the fact that the value $d = 200$ nm exceeds the critical diameter of the probe for the TM_{01} wave in the entire spectral range studied. Therefore, the transmission of this wave in the probe corresponds to the case of propagating waves, resulting in especially large values of T in the long-wavelength region.

A comparison with our previous results [20, 21] shows that the wavelength dependences of transmission of light in silicon and glass (or silica) waveguides are substantially different. The transmission coefficient of waveguides with a glass core monotonically increases with decreasing λ [20, 21]. At the same time, the transmission coefficient of probes with a silicon core first increases with decreasing λ_{max} in the IR region, achieving a maximum at a certain wavelength λ_{max}, and then drastically decreases for $\lambda \ll \lambda_{max}$ (see Figs 4 and 5). It is important that the transmission maximum is located in the visible spectral region between 550 and 800 nm.

Therefore, analysis of our results shows that transmission of a silicon probe is high both in the near-IR and visible regions if the probe length r_{in} does not exceed a few micrometres. For example, for $\lambda = 830$ nm, the cone angle $2\theta_0 = 60^\circ$ and $r_{in} = 2$ μm, we have $T = 1.9 \times 10^{-6}$, 4.8×10^{-4}, 6.4×10^{-3} and 8.5×10^{-2} for the exit-aperture diameters $d = 25$, 50, 70, and 100 nm, respectively. In the visible region at the He–Ne laser wavelength of 633 nm, the transmission coefficient of a silicon probe is two–three

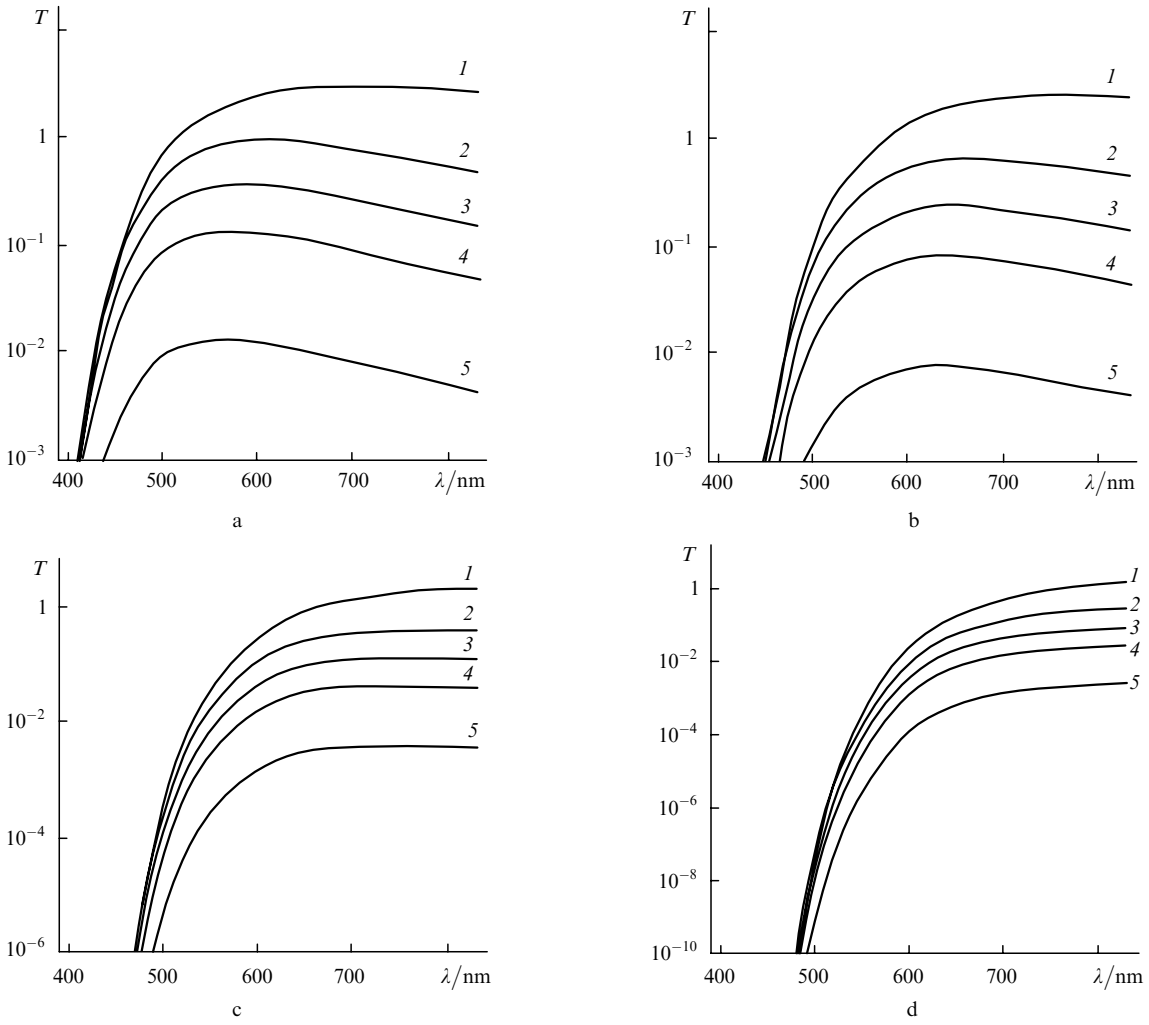

Figure 5. Same as in Fig. 4 for the cone angle $2\theta_0 = 120^\circ$ ($v = 1.777$).

orders of magnitude higher than that of a glass probe. It is equal to 1.6×10^{-5}, 3.6×10^{-3}, 4.1×10^{-2} and 3.9×10^{-1} for $d = 25$, 50, 70, and 100 nm, respectively, and the same cone angle $2\theta_0$ and waveguide length r_{in}. For an argon laser wavelength of 488 nm, we obtain $T = 9.4 \times 10^{-6}$, 1.6×10^{-3}, $1.2\times\ 10^{-2}$ and 4.5×10^{-2} for the same values of d, respectively. Note that, although absorption of light in silicon at this wavelength drastically increases, the transmission coefficient T of a silicon probe also considerably exceeds that of a metallised tapered glass probe.

As in the case of a glass waveguide, the transmission coefficient increases with increasing the cone angle (see Figs 4 and 5). As a result, for the angle $2\theta_0 = 120^\circ$, $\lambda = 633$ nm, and the same distance $r_{\text{in}} = 2$ μm from the cone apex to the probe entrance, we have $T = 7.6 \times 10^{-3}$, 8.0×10^{-2}, 2.3×10^{-1} and 6.2×10^{-1} for $d = 25$, 50, 70, and 100 nm, respectively.

A comparison with our recent calculations [20, 21] of the transmission coefficient of a metallised glass fibre ($n = 1.55$) suggests that the use of a silicon core in optical probes provides a significant increase in their transmission coefficient. For a specified cone angle, the advantages of silicon probes over glass or silica probes are especially revealed for small diameters of the exit aperture (i.e., under conditions providing a high spatial resolution of a near-field microscope). For example, for a probe of length $r_{\text{in}} = 2$ μm and the cone angle $2\theta_0 = 60^\circ$, the ratio $T_{\text{Si}}/T_{\text{glass}}$ of the transmission coefficients at 633 nm is 345, 620, 800, and 981 for the diameter $d = 100$, 70, 50, and 25 nm, respectively.

Another characteristic feature is that the transmission coefficient $T(\lambda)$ of a silicon probe for each fixed value of λ strongly decreases with increasing the probe length r_{in} (unlike a glass waveguide [20, 21]). As follows from our calculations, this dependence is relatively weak in the IR region and becomes rather strong in the short-wavelength part of the visible spectrum (see Figs 4 and 5). For example, as the probe length r_{in} increases from 2 to 10 μm, the transmission coefficient at $\lambda < 500$ nm decreases by a few orders of magnitude.

Note also the following circumstance. The consideration performed in the paper allows us to explain the physical reason for high transmission coefficients ($T > 1$), which can be obtained at large cone angles when the radius of the exit aperture is close to the critical one. This is related to a specific interference pattern of the field in the cone. For a certain combination of the wavelength of a light wave and geometrical parameters of the system, the integrated density of the field energy at the probe exit proves to be close to its peak value $W_{\text{tot}}^{\max}$, which can exceed substantially the corresponding values W_{tot} at the probe entrance (see Fig. 2).

Another reason for high transmission coefficients is related to the spherical wave front of optical fields considered in the cone. Unlike the case of a plane wave front, percolation of such fields through a tapered waveguide after reflection from its inclined walls is not accompanied by the transfer of energy of the fundamental wave to higher-order waves (which restricts transmission of light in the system [18]). Therefore, to provide high output energy densities of the field in practice, the input parameters of the field should be properly chosen. In particular, a converging initial wave front should be provided by focusing radiation coupled into a probe.

5. Conclusions

(i) We have developed the theoretical approach for calculating the spatial distribution of the energy density of the electromagnetic field in tapered optical probes filled with a medium with the complex permittivity. The approach is based on the consideration of spherical modes of a cone with the radial dependence suited for the description of the distribution of fields in optical probes with the subwavelength aperture. The specific case of the lowest-order TM_{01} mode was considered. The results of similar calculations for the dominating magnetic wave (the TE_{11} mode) will be published elsewhere.

(ii) The approach can be used at arbitrary cone angles of a tapered waveguide with the subwavelength aperture. It gives a clear picture of the behaviour of fields in an optical probe in a broad range of its geometrical parameters and wavelengths taking into account absorption of light and dispersion of the permittivity of the medium. The effect of dissipative losses in the core of a silicon probe on the radial distributions of the electric and magnetic energy densities was studied. It was found that the spatial distributions of the integrated density of the total electromagnetic energy in the short-wavelength and long-wavelength spectral regions are substantially different.

(iii) We have calculated the transmission coefficients of a metallised conical waveguide with a silicon core in the spectral region from 400 to 830 nm. As in the case of a metallised glass waveguide studied earlier, the calculations demonstrate strong dependences of the transmission coefficient on the exit aperture radius a, the cone angle $2\theta_0$, and the wavelength of light λ. The effect of absorption of light in silicon on the transmission coefficient of an optical probe was investigated.

(iv) The main differences between the calculated transmission of light in tapered optical waveguides with silicon and glass cores are caused by the following circumstances. First, absorption of light in silicon leads to an additional attenuation of the field percolated through a tapered probe. Therefore, the transmission coefficient in the short-wavelength region substantially depends on the probe length, unlike the case of glass fibres [20, 21]. On the other hand, the high refractive index of silicon compared to glass leads to a considerable decrease in the length of the part of a tapered waveguide where it operates in the supercritical regime. This significantly reduces the field attenuation in the supercritical part of the probe. The relative role of these factors in silicon strongly depends on the wavelength of light.

(v) Absorption of light in the near-IR region comparatively weakly affects the transmission coefficient of a tapered waveguide. Therefore, due to its high refractive index, silicon used in optical probes always has a great advantage over glass and silica because it provides high transmission of light. In the visible spectral range the transmission coefficient is strongly dependent on the length of the silicon probe. For waveguide lengths no more than a few micrometres, significant advantages of using silicon also become obvious. For example, if the probe length is ~ 2 μm and the cone angle is 60°, the transmission coefficient increases by a factor of $10^2 - 10^3$ in the 550 – 700-nm region compared to that for glass waveguides. However, if the probe length exceeds 8 – 10 μm, the transmission coefficient drastically decreases due to absorption of light in silicon. Therefore, in this case the advantage of silicon retains only in the long-wavelength part of the visible spectrum and in the IR region.

(vi) The main conclusion of the paper is that in the case of a proper choice of geometrical parameters of a silicon probe, refraction of light dominates over its absorption. For this reason, the use of probes with the silicon core in near-field microscopy provides the high transmission coefficients in the visible and near-IR regions along with a high spatial resolution. Note in conclusion that it is also interesting to apply the developed approach to other absorbing media with high refractive indices.

Acknowledgements. This work was supported by the scientific program Optical Spectroscopy and Frequency Standards, RAS, and the Russian Foundation for Basic Research (Grant No. 02-02-16274).

References

1. Betzig E., Trautman J.K., Harris T.D., Weiner J.S., Kostelak R.I. *Science*, **251**, 1468 (1991).
2. Pohl D.W. *Thin Solid Films*, **264**, 250 (1995).
3. Ohtsu M. (Ed.) *Near-Field Nano/Atom Optics and Technology* (Berlin: Springer-Verlag, 1998).
4. Noell W., Abraham M., Mayr K., Ruf A., Barenz J., Hollricher O., Marti O., Güthner P. *Appl. Phys. Lett.*, **70**, 1236 (1997).
5. Islam M.N., Zhao X.K., Said A.A., Mickel S.S., Vail C.F. *Appl. Phys. Lett.*, **71**, 2886 (1997).
6. Yatsui T., Kourogi M., Ohtsu M. *Appl. Phys. Lett.*, **71**, 1756 (1997); *Appl. Phys. Lett.*, **73**, 2090 (1998).
7. Eckert R., Freyland J.M., Gersen H., Heinzelmann H., Schürmann G., Noell W., Staufer U., de Rooij N.F. *Appl. Phys. Lett.*, **77**, 3695 (2000); *J. Microsc.*, **202**, 7 (2001).
8. Naber A., Molenda D., Fischer U.C., Maas H.J., Höppener C., Lu N., Fuchs H. *Phys. Rev. Lett.*, **89**, 21801 (2002).
9. Hecht B., Sick B., Wild U.P., Deckert V., Zenobi R., Martin O.J.F., Pohl D.W. *J. Chem. Phys.*, **112**, 7761 (2000).
10. Novotny L., Pohl D.W., Regli P. *J. Opt. Soc. Am. A*, **11**, 1768 (1994).
11. Novotny L., Pohl D.W., in *Photons and Local Probes*. Ed. by O. Marti, R. Möller (Dordrecht: NATO ASI Series E, Kluwer, 1995) p. 21.
12. Novotny L., Pohl D.W., Hecht B. *Opt. Lett.*, **20**, 970 (1995); *Ultramicroscopy*, **61**, 1 (1995).
13. Furukawa H., Kawata S. *Opt. Commun.*, **132**, 170 (1996).
14. Nakamura H., Sawada K., Kambe H., Saiki T., Sato T. *Prog. Theor. Phys. Supplement.*, **138**, 173 (2000).
15. Nakamura H., Sato T., Kambe H., Sawada K., Saiki T. *J. Microsc.*, **202**, 50 (2001).
16. Knoll B., Keilmann F. *Opt. Commun.*, **162**, 177 (1999).
17. Kuznetsova T.I., Lebedev V.S. *J. Russ. Laser Res.*, **22**, 123 (2001); *J. Russ. Laser Res.*, **23**, 211 (2002).
18. Kuznetsova T.I., Lebedev V.S. *Kvantovaya Elektron.*, **32**, 727 (2002) [*Quantum Electron.*, **32**, 727 (2002)].
19. Kuznetsova T.I., Lebedev V.S. *J. Russ. Laser Res.*, **24**, 458 (2003).

20. Kuznetsova T.I., Lebedev V.S. *Kvantovaya Elektron.*, **33**, 931 (2003) [*Quantum Electron.*, **33**, 931 (2003)].
21. Kuznetsova T.I., Lebedev V.S., Tsvelik A.M. *J. Opt. A: Pure and Appl. Opt.*, **6**, 338 (2004).
22. Danzebrink H.U., Castiaux A., Girard C., Bouju X., Wilkening G. *Ultramicroscopy*, **71**, 371 (1998).
23. Dziomba T., Danzebrink H.U., Lehrer C., Frey L., Sulzbach T., Ohlsson O. *J. Microsc.*, **202**, 22 (2001).
24. Yatsui T., Isumi K., Kourogi M., Ohtsu M. *Appl. Phys. Lett.*, **80**, 2257 (2002).
25. Castiaux A., Danzebrink H.U., Bouju X. *J. Appl. Phys.*, **84**, 52 (1998).
26. Hillenbrand R., Keilmann F. *Phys. Rev. Lett.*, **85**, 3029 (2000); *Appl. Phys. B*, **73**, 239 (2001).
27. Vainshtein L.A. *Elektromagnitnye volny* (Electromagnetic Waves) (Moscow: Radio i Svyaz', 1988).
28. Landau L.D., Lifshits E.M. *Electrodynamics of Continuous Media* (Oxford: Pergamon Press, 1960; Moscow: Nauka, 1982).
29. Abramowitz M., Stegun I.A. (Eds) *Handbook of Mathematical Functions* (New York: Dover, 1965; Moscow: Nauka, 1979).
30. Aspnes D.E., Studna A.A. *Phys. Rev. B*, **27**, 985 (1983).